The ultra–sensitive electrical detection of spin Rabi oscillation at paramagnetic defects

C. Boehme*, K. Lips

Hahn–Meitner–Institut Berlin, Kekulestrasse 5, 12489 Berlin, Germany

Abstract

A short review of the pulsed electrically detected magnetic resonance (pEDMR) experiment is presented. PEDMR allows the highly sensitive observation of coherent electron spin motion of charge carriers and defects in semiconductors by means of transient current measurements. The theoretical foundations, the experimental implementation, its sensitivity and its potential with regard to the investigation of electronic transitions in semiconductors are discussed. For the example of the P_b center at the crystalline silicon (111) to silicon dioxide interface it is shown experimentally how one can detect spin Rabi-oscillation, its dephasing, coherence decays and spin–coupling effects .

Key words: PACS: 71.55.-i 72.20.Jv 76.90.+d 72.25-b

* corresponding author

C. Boehme

Hahn–Meitner–Institut Berlin

Kekulestrasse 5, 12489 Berlin, Germany

tel +49-30-8062-1314; fax ++49-30-8062-1333

Email address: boehme@hmi.de (C. Boehme).

1 Introduction

Electron spin resonance (ESR) has proven in the past to be a useful characterization method for the microscopic investigation of paramagnetic semiconductor defects. The limitations of ESR spectroscopy on semiconductors is set by its sensitivity. Wavelengths in the microwave range are too long to be detected as single photons. Thus, as low dimensional semiconductors and mesoscopic structures such as quantum–wells, -dots or -wires or semiconductor thin films have increasingly become subjects of research, ESR spectroscopy with a sensitivity limit of the order of 10^{11} spins for the widely used X-Band ($\approx$ 10GHz) is hardly applicable anymore.

In order to achieve higher sensitivities, magnetic resonance methods have been combined in the past with other measurement techniques such as force microscopy (1), photoluminescence (2; 3) or conductivity measurements (4; 5) which have all reached single spin detection sensitivity in recent years. Among these methods, the electrically detected magnetic resonance (EDMR) techniques may be most beneficial for the spin spectroscopy of semiconductors since naturally, it is very sensitive to centers which influence conductivity while it is blind to all other spins. For most of the EDMR studies found in literature, including those reporting on a single spin detection, the experiments were conducted as pure continuous wave (cw) measurements; Pulsed (p) EDMR experiments have only been demonstrated recently (6; 7; 8). Since pEDMR combines the advantages of pulsed ESR with those of cw EDMR, these first results suggest that new insights can potentially be found for the many materials on which cw EDMR has been performed in the past. Beyond material spectroscopy, pEDMR is also expected to play a role for semicon-

ductor based quantum information concepts: So far, only electrical single spin detection but not electrical single spin readout experiments have been demonstrated (4; 5). A readout of a single spin requires a coherent spin measurement that allows to distinguish between different eigenstates. A requirement which can only be met by coherent spin–detection schemes as used for pEDMR experiments.

In the following, a brief review of the theoretical and experimental foundations of pEDMR experiments is given. It is shown how one can access coherent spin–Rabi oscillation by means of electric currents and how this observation can reveal new insights into the nature of the observed defect centers. The sensitivity limitations of pEDMR are addressed, too. As model system P_b centers at the crystalline silicon (c-Si) (111) interface to silicon dioxide (SiO_2) are used in order to show that qualitatively different electronic transitions can take place at identical defects.

2 Theoretical background

PEDMR takes advantage of the spin–dependency of charge carrier transitions in semiconductors which usually occurs when spin–conservation is imposed on electronic transitions. Spin–dependent transition rates between paramagnetic centers can be described in terms of a spin pair ensemble $\hat{\rho}$ consisting of pairs of two spins with $s = 1/2$ corresponding to the two states between which transitions occur (9; 10; 11). The transition rates will be proportional to the singlet content $[\hat{\rho}, |S\rangle\langle S|]^-$ and thus, by measuring currents as a function of time, the spin evolution of $\hat{\rho}$ can be accessed.

The challenge for pEDMR measurements is to detect very small current changes on top of comparatively large constant current offsets at a high time resolution. It is usually impossible to attain a time resolution with electrical measurements that is within the coherence time of the spin systems and that is at the same time sensitive enough to detect the subtle signal currents. This contradiction between sensitivity and time resolution is solved for pEDMR with an indirect detection scheme (12; 7; 11; 8; 13) where the change of the photocurrent after a coherent pESR excitation is measured as a function of the length of the resonant pulse. A sketch of this measurement principle is illustrated in fig. 7: The experiment begins when the steady state ensemble $\hat{\rho}^S$ that, due to the short singlet lifetimes, consists mainly of pure triplet eigenstates, is coherently manipulated and brought into a non–steady state, non–eigenstate $\hat{\rho}(\tau, B_1, \omega)$. After the excitation, the non–eigenstates will carry out a Larmor precession whose influence on the net transition rate will fade quickly due to the ensemble dephasing (14). Thus, a short time after the end of the microwave pulse, a non–steady state transition rate is present that relaxes slowly (on a μs to ms time scale) back to the steady state. It is known (11) that the integral of this relaxation current Q is proportional to the the density change

$$\Delta := -\frac{\rho_{11,44} - \rho^S_{11,44}}{\mathrm{Tr}\left[\rho^S\right]} = \frac{\rho_{22,33} - \rho^S_{22,33}}{\mathrm{Tr}\left[\rho^S\right]} \frac{\hbar\omega_\Delta}{\hbar\omega_\Delta \pm (J + D^d)}, \tag{1}$$

wherein ρ_{ii} and ρ^S_{ii} are the density matrix and the steady state density matrix elements, respectively and J, D^d and ω_Δ correspond to the exchange coupling, the dipolar coupling and the Larmor separation within the pairs, respectively (11; 7). Because of this, $\Delta = \Delta\left(\hat{\rho}(\tau), \hat{\rho}^S\right)$ is a function of the ensemble state $\hat{\rho}(\tau)$ right at the end of the pulse and thus, it is possible to

determine the evolution of $\hat{\rho}(\tau)$ during the excitation by measurement of Q as function of the pulse length τ. The time resolution of this measurement scheme if obviously not determined by the current amplifier but the pulse length generator and thus, a low ns–range time resolution is technically easy to achieve.

For the detection of spin–Rabi oscillation during the coherent excitation, $Q(\tau)$ must be recorded while the microwave field B_1 is strong enough so that Rabi frequencies can attain the higher MHz range and the microwave frequency ω is in ESR with a selected defect or impurity. A quantum mechanical description of this experiment (11) has revealed an expression

$$\Delta(\tau) = g_i \mu_B B_1 \Phi(\omega) \int_{-\infty}^{\infty} \frac{\sin^2\left(\kappa g_i \mu_B B_1 \tau \sqrt{1+x^2}\right)}{1+x^2} dx \qquad (2)$$

under the assumption of homogeneous B_1 fields and a sufficiently smooth line shape $\Phi(\omega)$ of the spin or spins in resonance which means $\partial_\omega \Phi(\omega_i) g_i \mu_B B_1 \ll \Phi(\omega)$. In eq. 2, pair partner i has a Landé–factor g_i and is exposed to an external magnetic field B_0 whereas κ denotes a factor whose value depends on the spin–spin couplings within a pair. An illustration of two of these coupling cases based on a theoretical calculation (11) is given in fig. 2. Weak coupling ($g_a - g_b \gg D, J$) implies that an ESR excitation can always manipulate either spin **a** or spin **b**, depending on the chosen excitation frequency ω. Hence, the Rabi oscillation reflects the transient nutation of a simple $s = 1/2$ electron spin and therefore, $\kappa = 1$. When the coupling is strong ($g_a - g_b \ll D, J$), the excitation is not selective for any pair partner anymore and hence, two $s = 1/2$ electron spins are turned and $\kappa = 2$. The simulated transients plotted in fig. 2 where calculated under negligence of incoherence. The decay of the oscillation is therefore due to the gradual spectral narrowing of the excitation

width with increasing pulse length.

In addition to the two coupling cases illustrated in fig. 2, another case shall be mentioned here: When $g_a - g_b \ll D, J$ (strong coupling) but $B_1 \ll J, D^d$, then $\kappa = \sqrt{2}$. While this case has so far not been described theoretically for pulsed EDMR experiments, one can deduce it from the description of transient nutation experiments of $s > 1/2$ systems without hyperfine influences as given by Astashkin and Schweiger (15).

3 A pEDMR experiment with Pb-centers

We have chosen recombination currents at the well understood and well characterized Pb-center to serve as a model system for the demonstration of pEDMR. P_b centers are trivalent silicon (Si) atoms at the c-Si/SiO_2 interface. They dominate interface trapping and recombination, they are paramagnetic when uncharged (16) and they are strongly localized, anisotropic electronic states (17). For the c-Si (111) surface orientation, all P_b centers point into a direction perpendicular to the interface. Because of this, their microscopic anisotropy is reflected by the ESR as well as EDMR spectra as shown repeatedly in the literature (17; 18). First pEDMR studies at the Pb-center have been carried out recently by Friedrich et al. (18) which revealed that charge carrier trapping and recombination can take place without the presence of additional shallow trapping centers through a two step trapping/readjustment direct capture process that had been described theoretically first by Shockley and Read (19) and later Rong et al. (20).

In order to conduct pEDMR, a semiconductor sample must be placed inside

a microwave resonator such that the B_1 field about the centers that are to be excited can be generated. Since electrical contacts naturally consist of conducting material, they may alter the eigenmodes of the microwave cavities whose geometry was designed under the assumption that the fill–factor of conducting material therein is negligible. The uncontrolled change of eigenmodes can lead to a strong inhomogeneity of the B_1 field throughout the resonator, especially at the sample position. This change of the B_1 modes is usually without any detrimental effect on cw EDMR measurements. However, for the detection of coherent spin motion during pEDMR experiments, a B_1 distribution will cause a rapid, artificially induced dephasing of the spins in resonance and thus, the observation of Rabi oscillation will become impossible. Thus, the sample and especially the contacts must be designed such that a B_1 distortion is as small as possible, which means that sample substrates should preferably be insulators and sample contacts must have thicknesses below the microwave penetration depth. The solution to this problem presents a complete thin film contact wiring of the sample within the microwave resonator as it is illustrated in fig. 3(a) to (c). In (a), a sketch of a thin film wired sample within a cylindrical microwave resonator is shown. While the actual semiconductor sample with its interdigited contact grid is located at the tip of the match–like substrate in the center of the cavity, it is connected to the contact pads on the outside by 40mm long and less than 200nm thin Al-stripes. Figure 3(b) displays a photo of a real thin film wire and contact structure. One can see the structure and its dimensions with contact pads, wires and grids. The grid area consists of 75 grid pairs where each grid has 5μm width and 15μm distance to its respective neighbors as indicated in fig. 3(c). With the sample and contact geometry given, one can (i) minimize sample resistances and therefore maximize sample currents, time resolution and sensitivity and (ii) the actual

semiconductor sample will be at the center of the cavity where the B_1 field has its maximum, while (iii) the eigenmodes of the cavity especially at its center remain undistorted.

The sample used for the experiment was made from a 380μm thick (111) surface oriented, slightly phosphorous doped ($\approx 10\Omega$cm) Czochralski grown c-Si Wafer whose surface was subjected to an RCA cleaning procedure followed by the formation of a 204nm thermal oxide layer. The oxide was formed at 1050^{o}C under exposure of the sample to O_2 for 200 min. The thickness of the resulting oxide was confirmed by profilometer measurements. After the oxide formation, the specially designed contact and wire system was deposited by means of a photolithographic lift–off procedure before the wafer was cut into match–like stripes. The current detection and coherent microwave excitation as well as the extraction of spin–dependent currents from microwave induced currents was executed with the same setup and the same procedure as described in Refs. (8) and (7).

All experiments presented in the following were performed at a sample temperature of $T = 10$K and a sample irradiation of 0.2(1)W/cm^2 with Ar^+ laser light with $\lambda = 514$nm wavelength. For the coherent excitation, a Bruker E580 X-Band pulse ESR spectrometer was used. A photocurrent of $I = 5\mu$A was established by a constant current source with long dwell time (1s) to allow a drift compensation. In order to measure the charge Q, the current was then subtracted by the constant offset before it was transformed by an impedance changer into a voltage signal which was then filtered by a high pass and subsequently digitized by an 8 bit transient recorder. The integration took place between 14μs and 30μs after the pulse which is the part of the photocurrent relaxation transient where the current signal reached its maximum.

The signal to noise ratios (SNR) per charge carrier pair, which poses an upper limit for the spin sensitivity since several charge carrier pairs can undergo transitions at one defect, was $\frac{SNR}{\mathrm{eh-pair}} = \frac{\sqrt{n}}{10^6}$ at 250W microwave power. Thus, within an 8 hour period and 300μs shot repetition time, one can attain a sensitivity of a few hundred charge carriers. This sensitivity is about 8 to 10 orders of magnitude higher than conventional ESR measurements, yet it is still not a single spin or even a single spin per single shot sensitivity. The reason for this limit is the presence of strong artifact currents within the sample due to the application of the strong microwave pulses. It is therefore not a principle limitation of the measurement method but due to the sample design. A further downscaling of the sample area and the prevention of shunt currents due to diffused excess charge carriers in the c-Si bulk could push the sensitivity even further.

4 Experimental results

We have recorded magnetic field sweeps of Q as a function of the strength of the external magnetic field B_0 as well as the angle between B_0 and the c-Si (111) orientation of the sample in order to confirm that the measured signals are due to electronic transitions at P_b centers. Figure 4(a) displays Q as a function of B_0 for a sample orientation of 90° which was recorded after an excitation with τ = 400ns pulse length and a microwave power of 4W. The data was fit with two Lorentzian line shapes (thick solid line). The fit results for each line are displayed by the thin lines. One can see that the fit marked as peak 1 has a much stronger intensity in comparison to the fit marked as peak 2. The measurement represented by fig. 4(a) was repeated for sample

orientations with angles of 60°, 30°, and 0°. In all cases, the data could be fit reasonably with two Lorentzians. The g–factor fit results of all four fits are displayed in fig. 4(b) and show that peak 1 has a clear anisotropy, while the smaller peak 2 has either no anisotropy or a much weaker anisotropy below the error margin of the fit results. The comparison of the fit results with the literature data of the P_b–center at the c-Si(111) surface (solid line) shows a clear agreement of the g-factors of peak 1 and hence, the signal associated with peak 1 is due to electronic transitions involving P_b–centers.

For the electrically detected spin–Rabi oscillation experiment, the sample orientation was turned back into the 90° position since then, the two peaks were well separated such that an excitation of peak 2 was minimized when the resonant excitation of peak 1 was maximized. The microwave frequency and the external field B_0 where adjusted such the the peak maximum at $g \approx 2.008$ was on resonance. The pulse length was then changed between $\tau = 0$ns and $\tau = 800$ns in 2ns steps. The measured results for Q as a function of the pulse lengths τ are displayed in fig. 5(a) and (c) for applied microwave powers of 250W and 64W, respectively, which correspond to arbitrary microwave fields $2B_1$ and B_1. One can clearly see the oscillatory behavior in both plots.

The maxima in the plots (a) and (c) of fig. 5 were fit with simple exponential decay functions. The two fits agree within the margin of error and reveal a time constant of ≈ 500ns. In order to determine the frequency components of the two data sets, they were subjected to fast Fourier transforms (FFT) whose absolute results are plotted in fig. 5(b) and (d) for the microwave field strengths of $2B_1$ and B_1, respectively. The data of both plots was fit with two Lorentzian functions (thick solid lines) whose individual fit results are represented by the thin solid lines and printed in the graphs.

5 Discussion of results

One can interpret the data presented ins figs. 4 and 5 by taking advantage of Rabis formula $\Omega = \sqrt{\kappa B_1^2 + (\omega - \omega_i)^2}$ (11), wherein ω is the exciting radiation frequency, ω_i the Larmor frequency of one or both pair partners, κ is the prefactor which depends on the coupling situation within the pair and B_1 field is expressed in gyromagnetic units. Note that $\Omega \propto B_1$ when we measure on resonance. Since this is exactly the case for the the lower frequencies Ω_L^1 and Ω_L^2 and the data was acquired at the maximum of peak 1 in fig. 4(a), one can conclude that the slowly decaying oscillation is solely due to spin–Rabi oscillation involving the P_b center. For the higher, broadly distributed frequencies centered around Ω_H^1 and Ω_H^2 this is different: From Rabis formula, we learn that when we measure off–resonant at arbitrary Rabi–frequencies Ω^1 and Ω^n with two different B_1 fields with ratio $B_1^1 = nB_1^2$, the Larmor–frequency difference can be calculated as

$$\omega_i - \omega = \sqrt{\frac{n^2\Omega^{1\,2} - \Omega^{n\,2}}{n^2 - 1}}. \tag{3}$$

With regard to the measurements of fig. 5 where $n = 2$, this means that $\omega - \omega_i = 16(10)\text{MHz} \simeq 0.6(4)\text{mT}$ and thus, we can conclude, that the process responsible for the fast dephasing signal can be associated with peak 2 of fig. 4(a) whose Larmor–frequency ω_2 was about 0.9mT higher than the excitation frequency ω. As a consequence one can conclude that the broad width of peak 2 may be due to a pair system consisting of the defect center associated with peak 2 and the P_b center. Since such a defect pair would be created at random distances, a broad distribution of transition times and thus the peak width would be expected. Microscopically, it is conceivable that an unrelaxed

E' centers, a so called EP/E'_δ in proximity of the interface may be the origin of the observed signal. Since this center is known to be a deep hole trap, the spin–dependent process would be a transition between neutral P_b and EP/E'_δ centers.

Another consequence of Rabis formula mentioned above is that when we have different components Ω_H and Ω_L in one measurement, we can obtain the ratio of their coupling factors

$$\frac{\kappa_H}{\kappa_L} = \sqrt{\frac{{\Omega_H^1}^2 - {\Omega_H^2}^2}{{\Omega_L^1}^2 - {\Omega_L^2}^2}} \tag{4}$$

from two measurements 1 and 2 collected at two arbitrary, different B_1 fields. Note that eq. 4 is independent of the Larmor–frequency difference which means it does not play a role whether any or both of the pair centers are on or off resonance. Thus, when the fit results of fig. 5(b) and (d) are plugged into eq. 4 we obtain $\frac{\kappa_H}{\kappa_L} = 1.31(27)$. With the properties associated with $\kappa = 1$, $\sqrt{2}$, and 2 as explained in section 2, this means that: (i) the B_1 field strength must have been larger than the Larmor separation of the pairs partners that belong to the peak 2 process. This is in accordance with the $B_1 \approx 1$mT strength that can be estimated from the width of peak 1 since it can only be due to power broadening and not due to incoherence or inhomgeneities because the latter two possibilities would also have broadened the peaks around Ω_L^1 and Ω_L^2 in the FFT plot of fig. 5(b) and (d). (ii) The coupling within the pairs associated with the P_b center must have narrowly distributed spin–exchange interactions beyond 10mT since spin–dipolar broadening of the peaks shown in fig. 4(a) can not be observed and the spin–spin interactions must exceed the estimated B_1 strength. Thus, the picture of a direct capture process of excess electrons into tightly coupled $P_b - e^-$ pairs as described by Ref. (18) is confirmed.

6 Summary

The ultra–sensitive electrical detection of electron spin–Rabi oscillation at P_b centers has been demonstrated and it was shown how new insights into the nature of charge carrier recombination at P_b can be gained. One can learn that there must be at least two qualitatively different recombination processes at P_b centers: (i) The direct capture recombination and (ii) a process with much shorter, strongly distributed transition times from a P_b centers to a second defect such as the EP/E'$_\delta$.

7 Acknowledgements

We thank Kerstin Jacob for the sample preparation and Kai Petter, Felice Friedrich, Walther Fuhs and Gerry Lucovsky for inspiring discussions

References

[1] D. Rugar and R. Budakian and H. J. Mamin and B. W. Chui, Nature (London) 430 (2004) 329.

[2] F. Jelezko and I. Popa and A. Gruber and C. Tiez and J. Wrachtrup and A. Nizovtsev and S. Kilin, Appl. Phys. Lett. 81 (12) (2002) 2160.

[3] F. Jelezko and T. Gaebel and I. Popa and A. Gruber and J. Wrachtrup, Phys. Rev. Lett. 92 (7) (2004) 076401–1.

[4] J. M. Elzerman and R. Hanson and L. H. Willems van Beveren and B. Witkamp and L. M. K. Vandersypen and L. P. Kouwenhoven, Nature (London) 430 (2004) 431.

[5] M. Xia and I. Martin and E. Yablonovitch and H. W. Jiang, Nature (London) 430 (2004) 435.

[6] I. Hiromitsu and Y. Kaimori and M. Kitano and T. Ito, Phys. Rev. B 59 (3) (1999) 2151–2163.

[7] Christoph Böhme, Dynamics of spin–dependent charge carrier recombination, Cuvillier Verlag, Göttingen, 2003.

[8] C. Boehme and K. Lips, Phys. Rev. Lett. 91 (24) (2003) 246603.

[9] D. Kaplan and I. Solomon and N. F. Mott, J. Phys. (Paris) – Lettres 39 (4) (1978) L51–L54.

[10] R. Haberkorn and W. Dietz, Solid State Commun. 35 (6) (1980) 505–508.

[11] C. Boehme and K. Lips, Phys. Rev. B 68 (24) (2003) 245105.

[12] C. Boehme and K. Lips, Appl. Phys. Lett. 79 (26) (2001) 4363–4365.

[13] C. Boehme and K. Lips, Appl. Magnetic Resonance 27 (2004) 109–122.

[14] C. Boehme and P. Kanschat and K. Lips, Europhys. Lett. 56 (5) (2001) 716–721.

[15] A. V. Astashkin and A. Schweiger, Chemical Physics Letters 174 (6) (1990) 595–602.

[16] Y. Nishi and T. Tanaka and A. Ohwada, Jpn. J. Appl. Phys. 11 (1972) 85.

[17] P. M. Lenahan and J. F. Conley, J. Vac. Sci. Technol. B 16 (1998) 2134–2153.

[18] F. Friedrich and C. Boehme and K. Lips, J. Appl. Phys. 97 (2005) 056101.

[19] W. Shockley and W. T. Read, Jr., Phys. Rev. 87 (5) (1952) 835.

[20] F. C. Rong and G. J. Gerardi and W. R. Buchwald and E.H. Poindexter and M. T. Umlor and D. J. Keeble and W. L. Warren, Appl. Phys. Lett. 60 (5) (1992) 610–612.

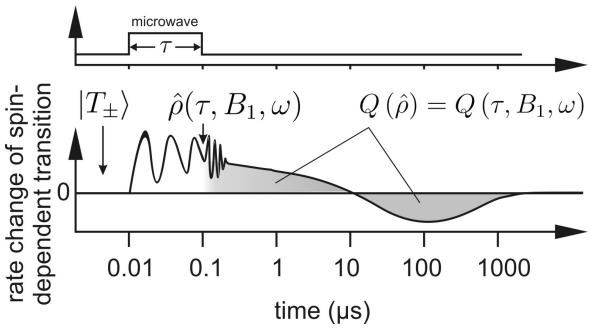

Fig. 1. The measurement principle of pEDMR on a logarithmic time scale. The integration of the transition rate Q after a coherent spin excitation is proportional to the singlet content of the ensemble state $\rho(\tau)$ at the end of the pulse. For details see text.

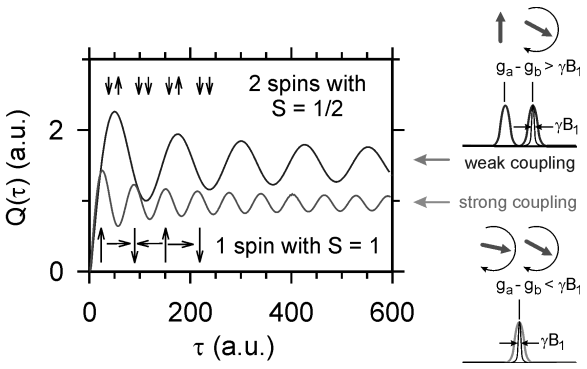

Fig. 2. Simulation of Q as a function of the pulse length τ for weak and strong spin–spin couplings. For details see text.

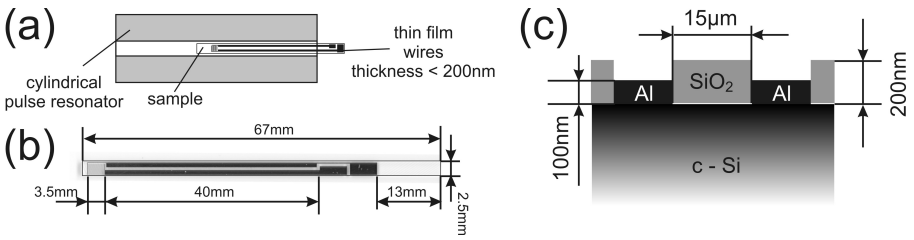

Fig. 3. (a) Sketch of a microwave mode compatible sample inserted in a dielectric microwave resonator. (b) Photo of a match like microwave mode compatible contact structure. (c) Sketch of the sample cross section with the c-Si/SiO_2 interface.

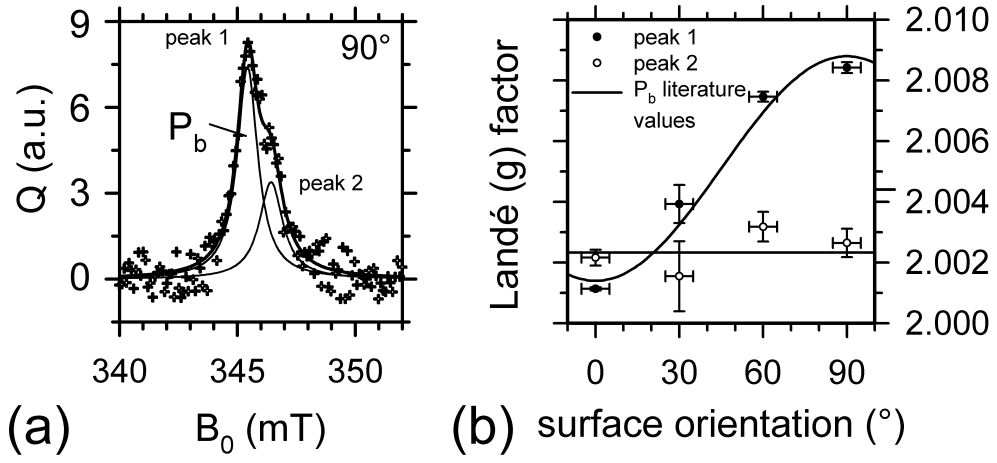

Fig. 4. (a) Measurement of $Q(B_0)$ for a sample orientation of 90° and a fit with two Lorentzian line shapes (solid line). (b) The g–factors of the two peaks observed in (a) as a function of the sample orientation.

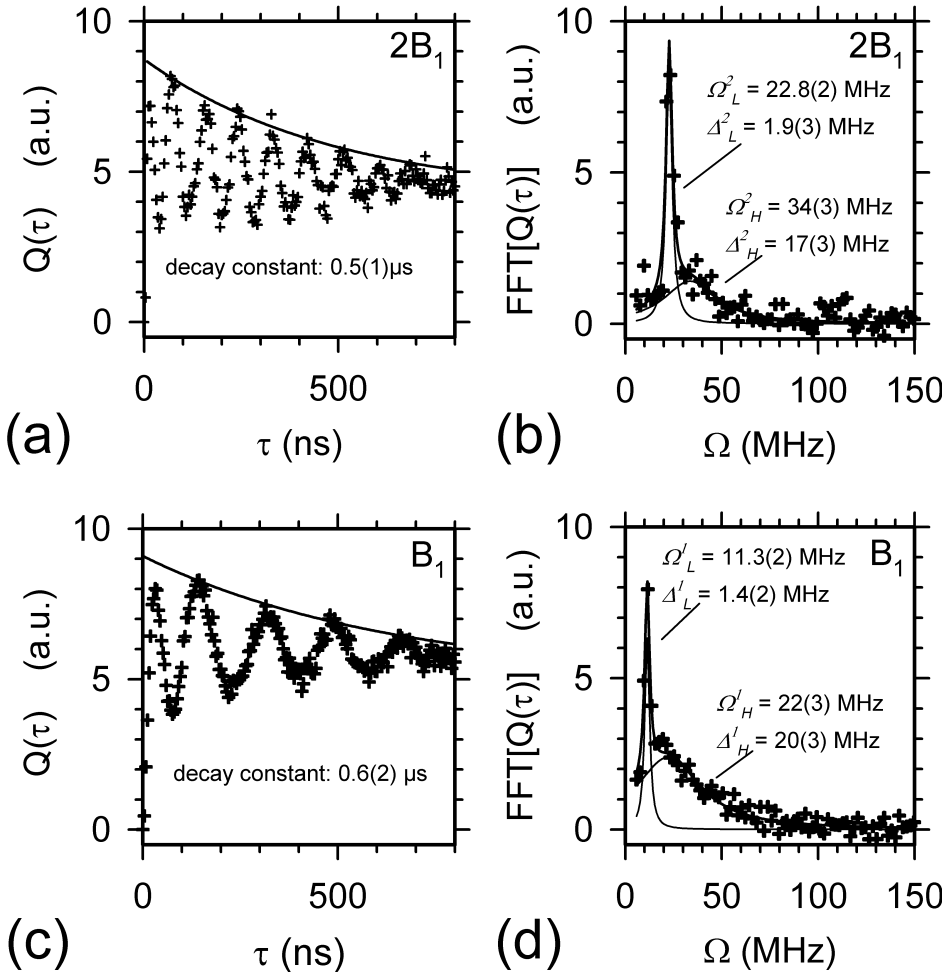

Fig. 5. (a) and (c): Measurement of $Q(\tau)$ for a sample orientation of 90° for two arbitrary microwave fields $2B_1$ and B_1, respectively. (b) and (d) The fast Fourier transform of the data in (a) and (c), respectively. For details see text.